

# Celestial Mechanics Notes Set 5: Symmetric Periodic Orbits of the Circular Restricted Three Body Problem and their Stable and Unstable Manifolds

J.D. Mireles James

December 22, 2006

## Contents

<b>1</b>	<b>Introduction:</b>	<b>1</b>
<b>2</b>	<b>Symmetry in the CRTBP</b>	<b>2</b>
2.1	Symmetric Orbits . . . . .	4
2.2	Symmetry Properties of the Manodromy Matrix . . . . .	5
<b>3</b>	<b>Halo Orbits in the CRTBP, and the Method of Differential Corrections</b>	<b>8</b>
3.1	Computation of a Halo Orbit . . . . .	8
3.2	The Family of Halo Orbits at $L_1$ . . . . .	16
3.3	Family of Halo Orbits at $L_2$ . . . . .	18
<b>4</b>	<b>Computing Stable and Unstable Manifolds of Periodic Orbits Through Linear Analysis</b>	<b>21</b>
4.1	The Stable and Unstable Manifolds of the $L_1$ Halo Orbit . . . . .	23
4.2	Other Periodic Orbits . . . . .	27
4.3	Stable and Unstable Manifolds of the Lyapunov Orbits . . . . .	27

## 1 Introduction:

In this set of notes systematic methods for locating periodic orbits in the circular restricted three body problem (**CRTBP**) are presented which take advantage of the symmetry of the problem and the method of differential corrections. A method for numerically computing the stable and unstable manifolds of unstable periodic orbits is developed as well. These ideas are applied to halo and Lyapunov orbits.

## 2 Symmetry in the CRTBP

It is not immediately clear that the **CRTBP** has any symmetry. The geometry of the configuration space is certainly symmetric with respect to rotation about the  $x$ -axis, as the two primaries lie there. Moreover the collinear libration points are on the  $x$ -axis and the equilateral libration points, while not on the  $x$ -axis, are symmetric with respect to it. Indeed, the potential function for the **CRTBP** depends only on the distance of a particle from the primaries so that it is symmetric with respect to the  $x$ -axis.

On the other hand, the equations of motion contain anti-symmetric terms due to the coriolis acceleration in the rotating frame. These terms would seem, at first to rule out any symmetry in the problem. Nevertheless, the following can be shown.

**Theorem 1** *Let  $\mathbf{x}_0 = (\mathbf{r}_0, \mathbf{v}_0) \in \mathbb{R}^6$  be a point in the phase space of the **CRTBP**, and  $\phi(\mathbf{x}_0, [0, T])$  be the trajectory curve obtained by flowing  $\mathbf{x}_0$  forward by time  $T$ . Also, let  $\mathbf{x}_f = \phi(\mathbf{x}_0, T)$ . Then*

$$\phi^*(A\mathbf{x}_f, [0, T]) \equiv A\phi(\mathbf{x}_f, [0, -T])$$

where

$$A = \begin{bmatrix} 1 & 0 & 0 & 0 & 0 & 0 \\ 0 & -1 & 0 & 0 & 0 & 0 \\ 0 & 0 & 1 & 0 & 0 & 0 \\ 0 & 0 & 0 & -1 & 0 & 0 \\ 0 & 0 & 0 & 0 & 1 & 0 \\ 0 & 0 & 0 & 0 & 0 & -1 \end{bmatrix}$$

solves the **CRTBP** with  $\phi^*(A\mathbf{x}_f, 0) = A\mathbf{x}_f$ , and  $\phi^*(A\mathbf{x}_f, T) = A\mathbf{x}_0$ .

The symmetry described here is not hard to picture. The theorem says that if the flow  $\phi$  takes  $\mathbf{x}_0$  to  $\mathbf{x}_f$  in time  $T$  along some path  $C$  in the configuration space, then it takes  $A\mathbf{x}_f$  to  $A\mathbf{x}_0$  in the same time, along a path  $C^*$  in configuration space which is just the reflection  $C^* = AC$  of  $C$  across the  $xz$ -plane with a time reversal along  $C$ .

**Proof:** That  $\phi(\mathbf{x}_0, [0, T])$  is a solution curve means that

$$\frac{d}{dt}\phi(\mathbf{x}_0, t) = f(\phi(\mathbf{x}_0, t))$$

for all  $t \in [0, T]$ , where  $f : \mathbb{R}^6 / \{-\mu\} \cup \{1 - \mu\} \rightarrow \mathbb{R}^6$  is the vector field of the **CRTBP**.

To establish the theorem, we have to show that the same is true of the function defined by

$$\phi^*(A\mathbf{x}_f, t) \equiv A\phi(\mathbf{x}_f, -t)$$

for  $t \in [0, T]$ . To do this we compute

$$\begin{aligned}\frac{d}{dt}\phi^*(A\mathbf{x}_f, t) &= \frac{d}{dt}A\phi(\mathbf{x}_f, -t) \\ &= A\frac{d}{dt}\phi(\mathbf{x}_f, -t)\end{aligned}$$

But  $\phi(\mathbf{x}_f, -t) = \phi(\mathbf{x}_0, T - t)$  for all  $t \in [0, T]$ , by the group properties of the flow. Then

$$\begin{aligned}\frac{d}{dt}\phi(\mathbf{x}_f, -t) &= \frac{d}{dt}\phi(\mathbf{x}_0, T - t) \\ &= -f(\phi(\mathbf{x}_0, T - t))\end{aligned}$$

where the minus sign is due to the time reversal. (The proof of this is in the first note set).

Now consider the effect of the transformation  $A$  on the vector field;

$$f(\phi^*(A\mathbf{x}_f, t)) \equiv f(A\phi(\mathbf{x}_f, -t)) \quad (1)$$

$$\begin{aligned}&= f(A\phi(\mathbf{x}_0, T - t)) \\ &= \begin{bmatrix} -\phi_4 \\ \phi_5 \\ -\phi_6 \\ \phi_1 + 2\phi_5 - \frac{1-\mu}{r_1^3}(\phi_1 + \mu) - \frac{\mu}{r_2^3}(\phi_1(1 - \mu)) \\ (-\phi_2) - 2(-\phi_4) - \frac{1-\mu}{r_1^3}(-\phi_2) - \frac{\mu}{r_2^3}(-\phi_2) \\ -\frac{1-\mu}{r_1^3}(\phi_3) - \frac{\mu}{r_2^3}(\phi_3) \end{bmatrix} \\ &= \begin{pmatrix} -1 & 0 & 0 & 0 & 0 & 0 \\ 0 & 1 & 0 & 0 & 0 & 0 \\ 0 & 0 & -1 & 0 & 0 & 0 \\ 0 & 0 & 0 & 1 & 0 & 0 \\ 0 & 0 & 0 & 0 & -1 & 0 \\ 0 & 0 & 0 & 0 & 0 & 1 \end{pmatrix} \begin{pmatrix} \phi_4 \\ \phi_5 \\ \phi_6 \\ \phi_1 + 2\phi_5 - \frac{1-\mu}{r_1^3}(\phi_1 + \mu) - \frac{\mu}{r_2^3}(\phi_1(1 - \mu)) \\ (\phi_2) - 2(\phi_4) - \frac{1-\mu}{r_1^3}(\phi_2) - \frac{\mu}{r_2^3}(\phi_2) \\ -\frac{1-\mu}{r_1^3}(\phi_3) - \frac{\mu}{r_2^3}(\phi_3) \end{pmatrix} \\ &= -Af(\phi(\mathbf{x}_0, T - t)) \quad (2)\end{aligned}$$

as

$$A\phi = \begin{bmatrix} \phi_1 \\ -\phi_2 \\ \phi_3 \\ -\phi_4 \\ \phi_5 \\ -\phi_6 \end{bmatrix}$$

and both  $r_1 = \sqrt{(\phi_1 + \mu)^2 + \phi_2^2 + \phi_3^3}$  and  $r_3 = \sqrt{(\phi_1 - (1 - \mu))^2 + \phi_2^2 + \phi_3^3}$  are independent of the sign of  $\phi_2$ .

Putting the pieces of the computation together, one has that

$$\begin{aligned} \frac{d}{dt}\phi^*(A\mathbf{x}_f, t) &= A \frac{d}{dt}\phi(\mathbf{x}_f, -t) \\ &= A(-f(\phi(\mathbf{x}_0, T - t))) \\ &= -Af(\phi(\mathbf{x}_0, T - t)) \\ &= f(\phi^*(A\mathbf{x}_f, t)) \end{aligned}$$

for all  $t \in [0, T]$ . But this is exactly what it means to say that  $\phi^*$  solves the **CRTBP** on  $[0, T]$ . Evaluating the solution at 0 and  $T$  gives

$$\phi^*(A\mathbf{x}_f, 0) = A\phi(\mathbf{x}_f, 0) = A\mathbf{x}_f$$

and

$$\phi^*(A\mathbf{x}_f, T) = A\phi(\mathbf{x}_f, T) = A\mathbf{x}_0$$

Then  $\phi^*$  solves the desired boundary value problem, and the theorem is complete.

□

## 2.1 Symmetric Orbits

The previous theorem turns out to be very useful for computing periodic orbits. Suppose that at time  $t = 0$  a trajectory  $\phi$  begins at a point  $\mathbf{x}_0 \in xz$ , where  $xz$  is the  $xz$ -plane. Further suppose that it's velocity at this time is normal to the plane; i.e. that it has no velocity in either the  $x$  or the  $z$  directions. Finally suppose that at some later time  $t = \tau$  the trajectory  $\phi$  returns to the  $xz$ -plane, with normal velocity in the opposite direction of it's initial velocity.

Then the orbit is  $T$ -periodic with  $T = 2\tau$ . To see this, let  $\mathbf{x}_0 \in xz$  be the initial condition, and  $\mathbf{x}_f = \phi(\mathbf{x}_0, \tau) \in xz$ . Then define

$$\phi^*(\mathbf{x}_f, t) = \phi(\mathbf{x}_0, \tau + t)$$

Note that because  $\mathbf{x}_0$  and  $\mathbf{x}_f$  are in the  $xz$ -plane, we have that  $A\mathbf{x}_0 = \mathbf{x}_0$  and  $A\mathbf{x}_f = \mathbf{x}_f$ . ( $A$  fixes this entire plane). Then

$$\phi^*(\mathbf{x}_f, t) = \phi^*(A\mathbf{x}_f, t)$$

and by the previous theorem (combined with the existence and uniqueness theorem for flows)

$$\phi^*(A\mathbf{x}_f, t) = A\phi(\mathbf{x}_f, -t)$$

with  $\phi^*(A\mathbf{x}_f, 0) = A\mathbf{x}_f = \mathbf{x}_f$ , and  $\phi^*(A\mathbf{x}_f, \tau) = A\mathbf{x}_0 = \mathbf{x}_0$ .  $\phi^*$  is merely the reflection of  $\phi$  about the  $xz$ -plane (with a time reversal). Further since  $\phi(\mathbf{x}_0, \tau + t) = \phi^*(\mathbf{x}_f, t)$  by definition, it follows that

$$\phi(\mathbf{x}_0, 2\tau) = \phi^*(\mathbf{x}_f, \tau) = \mathbf{x}_0$$

so that  $\phi$  is indeed a  $2\tau$  periodic orbit. Since it's path in configuration space is just  $\phi$  and it's reflection about the  $xz$ -plane, it is a symmetric orbit.

These conditions will be used to compute symmetric periodic orbits later in the notes. This is done by choosing initial conditions in the  $xz$ -plane which satisfy the symmetry conditions, and then integrating until trajectory returns to the plane with the opposite orientation. This orbit can be used as the 'initial guess' for a Newton procedure, where the target state is as above; namely that the orbit returns to the  $xz$ -plane with normal velocity.

In such a procedure the  $x$ ,  $z$ ,  $\dot{y}$ , and  $\tau$  parameters can vary with  $x = 0$ ,  $z = 0$ ,  $\dot{x} = 0$ , and  $\dot{z} = 0$  as the target. This is developed fully later in the notes. First we derive a symmetry property of the manodromy matrix which will aid in the Newton computation, as the necessary differential in the Newton method depends on the manodromy matrix.

## 2.2 Symmetry Properties of the Manodromy Matrix

The symmetry theorem for the **CRTBP** shows that if an orbit satisfies certain symmetry conditions, then it is periodic. In this case, a symmetric periodic orbit is determined by it's half orbit. It is reasonable then, that the manodromy matrix of the full orbit would depend on the state transition matrix of the half orbit. In this section we show that;

**Theorem 2** *Let  $\mathbf{x}_0$ ,  $\mathbf{x}_f$ , and  $\tau$  be as above. Then the manodromy matrix  $\Phi(0, T)$  associated with  $\phi(\mathbf{x}_0, [0, T])$  is given by*

$$\Phi(0, T) = AJ\Phi(0, \tau)^T J^{-1} A\Phi(0, \tau)$$

where  $T = 2\tau$ .

(See Note Set 2 for the definition of  $\Phi$  and it's basic properties).

**Proof:**  $\Phi$  is the solution of the variational equations, and as such is itself a flow. Then

$$\Phi(0, T) = \Phi(-\tau, 0) \circ \Phi(0, \tau)$$

We begin by choosing a  $\mathbf{y}_0 \in B(\mathbf{x}_0, \epsilon)$  (in the argument that follows it is not necessary that  $\epsilon$  be small, but it may help to picture things this way. This is because, while the linear mapping  $\Phi(0, \tau)$  can act on any vector in  $\mathbb{R}^6$ , it is only a good linear approximation of  $\phi(\mathbf{x}_0, \tau)$  for  $\mathbf{y}_0$  near  $\mathbf{x}_0$ ). Then define

$$\mathbf{y}_1 = \Phi(0, \tau)\mathbf{y}_0$$

Recall that  $\mathbf{x}_0$  and  $\Phi(0, \tau)\mathbf{x}_0 = \mathbf{x}_f$  are on the  $xz$ -plane, so  $B(\mathbf{x}_0, \epsilon)$  is a symmetric neighborhood. Then  $\mathbf{y}_1$  lies in a symmetric neighborhood of  $\mathbf{x}_f$

Now define the reflections

$$A\mathbf{y}_0 \equiv \mathbf{y}_0^*$$

and

$$A\mathbf{y}_1 \equiv \mathbf{y}_1^*$$

Observe that  $A$  is its own inverse, so that

$$A\mathbf{y}_0^* = \mathbf{y}_0$$

and

$$A\mathbf{y}_1^* = \mathbf{y}_1$$

as well. Inserting this into the definition of  $\mathbf{y}_1$  gives

$$\Phi(0, \tau)A\mathbf{y}_0^* = A\mathbf{y}_1^*$$

or

$$\mathbf{y}_1^* = A\Phi(0, \tau)A\mathbf{y}_0^*$$

We claim that

$$\mathbf{y}_0^* = \Phi(-\tau, 0)\mathbf{y}_1^* \tag{3}$$

To see this note that  $\phi(\mathbf{x}_f, -\tau)$  is the inverse of  $\phi(\mathbf{x}_0, \tau)$ . (Compose these maps to check this). Now, consider the two Taylor expansions of  $\phi(\mathbf{y}_1^*)$  about  $\mathbf{x}_1^*$ . First

$$\begin{aligned} \phi(\mathbf{y}_1^*, \tau) &= \mathbf{x}_1^* + \Phi(-\tau, 0)\mathbf{y}_1^* + o(\mathbf{y}_1^*) \\ &= A\mathbf{x}_1 + \Phi(-\tau, 0)A\mathbf{y}_1 + o(A\mathbf{y}_1) \\ &= \mathbf{x}_1 + \Phi(-\tau, 0)A\mathbf{y}_1 + o(A\mathbf{y}_1) \end{aligned}$$

Similarly, using the symmetry relation  $\phi(\mathbf{y}_1^*, \tau) = A\phi(\mathbf{y}_1, -\tau)$  we also have

$$\begin{aligned} \phi(\mathbf{y}_1^*, \tau) &= A\phi(\mathbf{y}_1, -\tau) \\ &= A[\mathbf{x}_1 + \Phi^{-1}(0, \tau)\mathbf{y}_1 + o(\mathbf{y}_1)] \\ &= A\mathbf{x}_1 + A\Phi^{-1}(0, \tau)\mathbf{y}_1 + Ao(\mathbf{y}_1) \\ &= \mathbf{x}_1 + A\Phi^{-1}(0, \tau)\mathbf{y}_1 + Ao(\mathbf{y}_1) \end{aligned}$$

But these are the same expansions, and what's more since derivatives are unique, we can match like powers, at least up to the remainders. From this we have

$$\Phi(-\tau, 0)A\mathbf{y}_1 = A\Phi^{-1}(0, \tau)\mathbf{y}_1$$

Acting on  $\mathbf{y}_0^*$  gives

$$\begin{aligned}\Phi(-\tau, 0)\mathbf{y}_1^* &= \Phi(-\tau, 0)A\mathbf{y}_1 \\ &= A[\Phi^{-1}(0, \tau)\mathbf{y}_1] \\ &= A(\mathbf{y}_0) \\ &= \mathbf{y}_0^*\end{aligned}$$

which gives the claim. Having established it the theorem follows from  $\mathbf{y}_1^* = A\Phi(0, \tau)A\mathbf{y}_0^*$  and that

$$\mathbf{y}_0^* = A\Phi^{-1}(0, \tau)A\mathbf{y}_1^*$$

Using these, we have

$$\Phi(-\tau, 0)\mathbf{y}_1^* = A\Phi^{-1}(0, \tau)A\mathbf{y}_1^*$$

or

$$\Phi(-\tau, 0) = A\Phi^{-1}(0, \tau)A$$

Recalling that in the **CRTBP** the matrix  $\Phi$  is symplectic with respect to

$$J = \begin{pmatrix} 0 & I \\ -I & K \end{pmatrix}$$

where

$$K = \begin{pmatrix} 0 & 2 & 0 \\ -2 & 0 & 0 \\ 0 & 0 & 0 \end{pmatrix}$$

it is the case that

$$\Phi^{-1}(0, \tau) = J\Phi(0, \tau)^T J^{-1}$$

Finally

$$\begin{aligned}\Phi(0, T) &= \Phi(-\tau, 0) \circ \Phi(0, \tau) \\ &= AJ\Phi(0, \tau)^T J^{-1}A\Phi(0, \tau)\end{aligned}$$

□

This theorem gives a computationally efficient method for computing the the monodromy matrix of a symmetric orbit based only on knowledge of it's half orbit. This will be useful in the applications to follow, where we develop a Newton method for finding symmetric half orbits. The theorem says that computing the stability of the resulting full orbit does not require the computation of the full orbit.

### 3 Halo Orbits in the CRTBP, and the Method of Differential Corrections

A halo orbit is a periodic orbit in the **CRTBP** which is out of plan near  $L_1$ . The halo orbits do not exist in the linearization about  $L_1$ , but are a fully nonlinear phenomenon.

From the point of view of an observer on earth (or on the secondary body in the **CRTBP**) a satellite or projectile in one of these orbits looks as though it is orbiting the primary, or tracing a halo about the primary. However the halo orbits are typically quite far from the primary, in the 'neck' of the jacobi surface.

Then a halo orbit is an ideal location for studying solar winds, as a satellite placed there will always have clear line of sight with both the earth and the sun, yet because of the halo like property, will never pass directly between the earth and the sun. From the point of view of an observer on the earth this means the satellite never passes through the disk of the sun, where communications would be lost. (This is why placing such an observatory at  $L_1$  is impractical; communication with such an observatory would be impossible!). NASA has made use of these orbits in several missions including the 'Solar and Heliospheric Observatory' (SOHO) mission, and the Genesis mission.

#### 3.1 Computation of a Halo Orbit

The question of how one knows halo orbits exist and how to find them is a fascinating story. An excellent reference for the theory and design of halo orbits is [J]. Briefly one considers the dynamics near  $L_1$ .

The linearized model tells you that  $L_1$  has the *center*  $\times$  *center*  $\times$  *saddle* stability. However, as is well know, the linear model is insufficient for making accurate studies of the dynamics in the center. For this, normal forms are necessary. (A normal form is a polynomial approximation of the Hamiltonian).

The unstable dynamics can be decoupled from the center dynamics near the libration point by computing a normal form for the Hamiltonian of the **CRTBP** about  $L_1$  to some desired (high) order. The resulting dynamical system is numerically integrating and a Poincare section is chosen. If the order of the

normal form is high enough, this will give a good approximation of the dynamics in the center manifold in a large neighborhood of  $L_1$ .

Restricting the dynamics of the center manifold of  $L_1$ , one has a 4 dimensional dynamical system. Fixing an energy level (value for the Jacobi integral) reduces the dynamics to 3 dimensions. Finally, considering Poincare sections of the 3 dimensional flow gives a two dimensional dynamical system.

Examining the Poincare sections so obtained suggests that out of plane periodic orbits exist a substantial distance from the libration point. These orbits appear as fixed points of the Poincare section. Beginning with the coordinates of the fixed point of the Poincare section as an initial guess, one can return to the full **CRTBP** and use a Newton Method to search for the halo orbit.

Again, all of this is described in great detail in [J]. In this section, what we will assume is that we have been told that Halo Orbits exist in the **CRTBP**, and in fact that one can be found roughly  $1,200,000km$  from the earth, in the direction of the sun. The orbit has ‘radius’ roughly  $280,000km$ , for a projectile traveling roughly  $0.350km/sec$ . (Imagine this is rough data from either the Genesis or SOHO missions). In a later section we will present a method that can be used to find and compute families of halo orbits about any collinear libration for any value of  $\mu$ . But for now lets assume that we have only approximate physical data as to the location of a specific halo orbit in the Earth/Sun model.

To convert this data to the dimensionless coordinates of the **CRTBP** we use the fact that in metric units the distance from the earth to the sun (secondary to primary) is  $1Au = 1.496 * 10^8 km$  and the time it takes the secondary to orbit the primary is  $365.25days$ , while in the **CRTBP** the distance between the primaries is 1 and the period is  $2\pi$ . Then

$$1,200,000km \times \frac{1Au}{1.496 * 10^8 km} \approx 0.00802Au,$$

$$280,000km \times \frac{1Au}{1.496 * 10^8 km} \approx 0.00187Au$$

and

$$0.35 \frac{km}{sec} \times \frac{1Au}{1.496 * 10^8 km} \times \frac{31557600sec}{year} \times \frac{1year}{2\pi tu} \approx 0.0118Au/tu$$

where for the moment we take  $Au$  and  $tu$  to be the units of the **CRTBP** (these are in fact dimensionless, like radians).

Since the  $1,200,000km$  is measured from the earth, but the coordinates of the **CRTBP** are centered at the center of mass, we use the fact that the location of the secondary is  $1 - \mu$ , where here  $GM_{sun} = 1.327 * 10^{11} km^3/sec^2$  and  $GM_{earth} = 4.035 * 10^5 km^3/sec^2$  so that

$$\mu = \frac{GM_{earth}}{GM_{sun} + GM_{earth}} \approx 3.05 * 10^{-6}$$

We will use the symmetries of the **CRTBP** to target the orbit. We begin with an initial condition in the  $xz$ -plan, with no initial  $x$  or  $z$  velocity and

satisfying the conditions above. We target a final state which returns, after time  $\tau$  to the  $xz$ -plane, arriving with no  $x$  or  $z$  velocity. If we find such a half orbit then the symmetry of the **CRTBP** tells us that integrating from the initial position, backward in time by  $\tau$  will bring us to the same final condition. Then simply integrating from the initial position over a time  $2\tau$  will return us to the initial position, and we would have a periodic orbit.

We formalize this as follows. Our initial guess, in the coordinates of the **CRTBP**, is

$$\begin{aligned} x_0 &= 1 - \mu - 0.00802 \\ y_0 &= 0 \\ z_0 &= -0.00187 \\ \dot{x}_0 &= \\ \dot{y}_0 &= -0.0118 \\ \dot{z}_0 &= 0 \end{aligned}$$

as we are told that the projectile will appear to orbit the sun in a clockwise fashion when viewed by an observer on the earth.

We will hold the  $x_0$  coordinate fixed and search for  $z_0^*$ ,  $y_0^*$ , and  $\tau^*$  such that  $\dot{x}^*(\tau^*)$ ,  $\dot{z}^*(\tau^*)$ , and  $y^*(\tau^*)$  are all zero.

Define  $f : \mathbb{R}^3 \rightarrow \mathbb{R}^3$  by

$$f(z, \dot{y}, \tau) = \begin{bmatrix} \phi_4(x_0, 0, z, 0, \dot{y}, 0, \tau) \\ \phi_6(x_0, 0, z, 0, \dot{y}, 0, \tau) \\ \phi_2(x_0, 0, z, 0, \dot{y}, 0, \tau) \end{bmatrix}$$

where

$$\phi(x, y, z, \dot{x}, \dot{y}, \dot{z}, \tau) = \begin{bmatrix} \phi_1(x, y, z, \dot{x}, \dot{y}, \dot{z}, \tau) \\ \phi_2(x, y, z, \dot{x}, \dot{y}, \dot{z}, \tau) \\ \phi_3(x, y, z, \dot{x}, \dot{y}, \dot{z}, \tau) \\ \phi_4(x, y, z, \dot{x}, \dot{y}, \dot{z}, \tau) \\ \phi_5(x, y, z, \dot{x}, \dot{y}, \dot{z}, \tau) \\ \phi_6(x, y, z, \dot{x}, \dot{y}, \dot{z}, \tau) \end{bmatrix}$$

with  $\phi : U \subset \mathbb{R}^6 \rightarrow \mathbb{R}^6$  the flow generated by the **CRTBP**. Here we are treating  $x, y, z, \dot{x}, \dot{y}, \dot{z}$ , and  $\tau$  as independent variables, and define

$$U = \mathbb{R}^6 \setminus \{-\mu, 0, 0, 0, 0, 0\} \cup \{1 - \mu, 0, 0, 0, 0, 0\}.$$

To find the initial conditions for the halo orbit it is sufficient to find  $\mathbf{x}^* = (z_0^*, \dot{y}_0^*, \tau^*)^T$  satisfying the equation

$$f(z_0^*, \dot{y}_0^*, \tau^*) = \begin{bmatrix} 0 \\ 0 \\ 0 \end{bmatrix}$$

A Newton method for this problem is

$$\mathbf{x}_{n+1} = \mathbf{x}_n - [Df(\mathbf{x}_n)]^{-1}f(\mathbf{x}_n)$$

with  $\mathbf{x} = (z, \dot{y}, \tau)$  and  $\mathbf{x}_0 = (z_0, \dot{y}_0, \tau_0)$ . Here  $(z_0, \dot{y}_0, \tau_0)$  is the initial guess as to the whereabouts of the halo orbit (coming presumably from experimental data).

The differential is

$$\begin{aligned} Df(\mathbf{x}) &= \begin{bmatrix} \frac{\partial}{\partial z}\phi_4 & \frac{\partial}{\partial \dot{y}}\phi_4 & \frac{\partial}{\partial \tau}\phi_4 \\ \frac{\partial}{\partial z}\phi_6 & \frac{\partial}{\partial \dot{y}}\phi_6 & \frac{\partial}{\partial \tau}\phi_6 \\ \frac{\partial}{\partial z}\phi_2 & \frac{\partial}{\partial \dot{y}}\phi_2 & \frac{\partial}{\partial \tau}\phi_2 \end{bmatrix} \\ &= \begin{bmatrix} \Phi_{(4,3)} & \Phi_{(4,5)} & g_4(x_0, 0, z(\tau), 0, \dot{y}(\tau), 0) \\ \Phi_{(6,3)} & \Phi_{(6,5)} & g_6(x_0, 0, z(\tau), 0, \dot{y}(\tau), 0) \\ \Phi_{(2,3)} & \Phi_{(2,5)} & g_2(x_0, 0, z(\tau), 0, \dot{y}(\tau), 0) \end{bmatrix} \end{aligned}$$

where  $g : U \subset \mathbb{R}^6 \rightarrow \mathbb{R}^6$  is the vector field for the **CRTBP**;

$$\begin{aligned} g(x, y, z, \dot{x}, \dot{y}, \dot{z}) &= \begin{bmatrix} g_1(x, y, z, \dot{x}, \dot{y}, \dot{z}) \\ g_2(x, y, z, \dot{x}, \dot{y}, \dot{z}) \\ g_3(x, y, z, \dot{x}, \dot{y}, \dot{z}) \\ g_4(x, y, z, \dot{x}, \dot{y}, \dot{z}) \\ g_5(x, y, z, \dot{x}, \dot{y}, \dot{z}) \\ g_6(x, y, z, \dot{x}, \dot{y}, \dot{z}) \end{bmatrix} \\ &= \begin{bmatrix} \dot{x} \\ \dot{y} \\ \dot{z} \\ 2\dot{y} + D_x U \\ -2\dot{x} + D_y U \\ D_z U \end{bmatrix} \end{aligned}$$

and  $z(\tau) = \phi_3(x_0, 0, z, 0, \dot{y}, 0, \tau)$ ,  $\dot{y}(\tau) = \phi_5(x_0, 0, z, 0, \dot{y}, 0, \tau)$ . With these pieces in place we hope that if  $\mathbf{x}_0$  is close enough to the halo orbit, then  $\mathbf{x}_n \rightarrow \mathbf{x}^*$  as  $n \rightarrow \infty$ .

Also note that  $\tau_0$  is not given and must be determined. A good starting estimate  $\tau_0$  of  $\tau^*$  is obtained as follows. Integrate the given initial data. The resulting trajectory moves in the negative  $y$  direction away from the  $xz$ -plane, while  $z$  increases. We integrate until the trajectory returns to the plane. The time at which this occurs is our  $\tau_0$ . The situation is shown in Fig 1.

This can be done with a computer program, or simply with a little experimentation with the initial data. We found that at time  $t = 1.45$ ,  $y(t) \approx 1.9839e - 4$  and take  $\tau_0 = t$ .

Then we have all the necessary pieces to begin the Newton method. The program *haloNewton3* implements the method. After 14 iterations we find

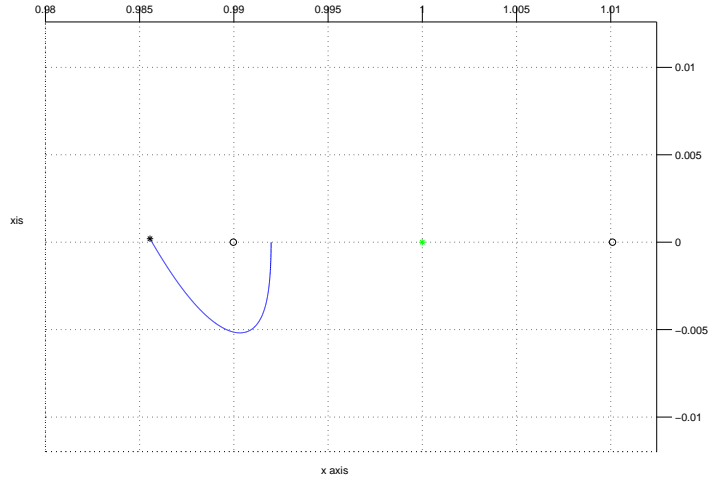


Figure 1: The initial trajectory

$$\begin{aligned}
 z_0^* &= -0.00191718187218 \\
 \dot{y}_0^* &= -0.01102950210737 \\
 \tau^* &= 1.52776735363559
 \end{aligned}$$

which gives the initial conditions

$$\mathbf{x}_{halo} = \begin{pmatrix} 0.9919755537727 \\ 0 \\ -0.00191718187218 \\ 0 \\ -0.01102950210737 \\ 0 \end{pmatrix}$$

and the period  $T = 2\tau^* = 3.05553470727118$ . We integrate these initial conditions over this period and the orbit shown in Fig 2 and Fig 3. The results show that we have indeed found the halo orbit. It is shown in blue while the trajectory of the initial guess is black.

The difference between the initial and final conditions of the orbit are roughly  $2.57e - 13$ , which gives a measure of the degree to which the numerically computed orbit is actually periodic. Then the problem is solved to thirteen significant figures.

The energy of the halo orbit is  $C_{halo} = 3.00079710038642$ . The halo orbit and the zero velocity curve are shown in Fig 4, (again the initial guess trajectory is black).

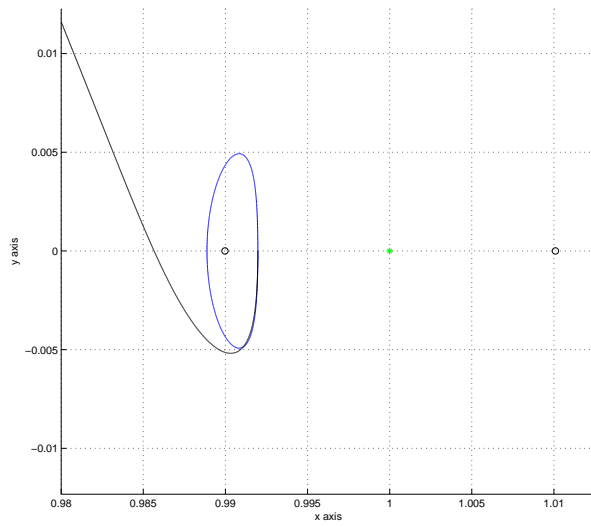


Figure 2: Top View of the Halo Orbit

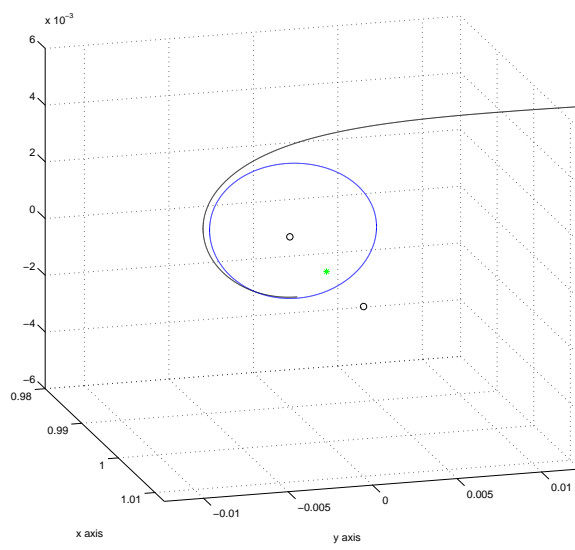


Figure 3: Front View of the Halo Orbit

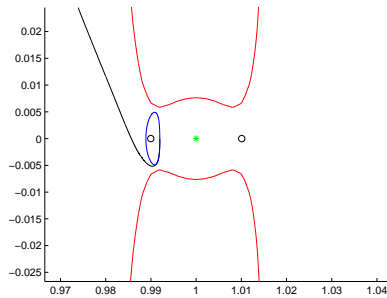


Figure 4: The Halo Orbit and it's Zero Velocity Surface

We can see the the Halo Orbit sits in the neck and goes around  $L_1$ . The initial conditions, in physical units, lie no less than a million kilometers from the earth. But we see that the halo is at least as wide as it is far from the earth. So the orbit is quite large and it's period is just a little under a half a year.

Now we consider the stability of the orbit. The programs *GCRTBP.m*, *stateTransCRTBP.m*, and *sysSolveCRTBP.m* solve the differential equation

$$\dot{\Phi} = Dg\Phi \quad \Phi(t_0, t_0) = \mathbf{I}$$

from time  $t = t_0$  through  $t = t_f$ . We use the halo orbit for the reference orbit and  $t_0 = 0$ ,  $t_f = T$  to obtain the monodromy matrix  $\Phi(0, T)$  for the halo orbit.

The monodromy matrix of a trajectory of a time invariant vector field will always have one as an eigenvalue. Further, for a generic orbit in a Hamiltonian system, the monodromy will always have a second eigenvalue of one. Both of these are due to the non-uniqueness of periodic orbits in Hamiltonian systems.

The first unity eigenvalue has an associated eigenvector which points in the direction of the flow (so is a tangent vector to the periodic orbit). The non-uniqueness here is due to the trivial fact that any point on a periodic orbit is a periodic point for the flow. (At each point on the trajectory we could begin a periodic orbit. All the curves so obtained are of course identical).

The second unity eigenvalue is due to a less trivial phenomenon. The eigenvector corresponding to this eigenvalue points in the direction of change in energy. To put it another way, every point in a Hamiltonian system has an associated energy (or first integral. Basically this is just the fact that the Hamiltonian is conserved along trajectories. This is an 'energy like' quantity, and we often abuse the language a little and just call it energy). The energy along the trajectory of that point is of course constant, but this will typically not be the only orbit with a given energy. Each fixed energy level defines a co-dimension one submanifold of the phase space so unless the phase space is two dimensional each such submanifold will contain many orbits. The eigenvector associated to the second unity eigenvalue is normal to the energy surface of the periodic orbit

(this is discussed in more detail in the section on the family of halo orbits near  $L_2$ ).

The remaining eigenvalues are the eigenvalues of the linearization of the Poincare map associated with the periodic orbit, restricted to the orbits energy level. Then the remaining eigenvalues describe, up to first order, the dynamics near the orbit (as the dynamics near the orbit are topologically conjugate to the dynamics of the Poincare section, and the dynamics of the Poincare section are locally topologically conjugate to the dynamics of it's linearization). An excellent reference is [MH]. This was also described in somewhat more detail in the last section of the previous set of notes.

Computing the monodromy matrix for the halo orbit gives

$$\Phi(0, T) \approx 10^3 \begin{pmatrix} 1.132 & -0.026 & 0.191 & 0.232 & 0.213 & 0.026 \\ -1.042 & 0.025 & -0.176 & -0.213 & -0.196 & -0.024 \\ 0.127 & -0.003 & 0.022 & 0.026 & 0.024 & 0.003 \\ 3.454 & -0.080 & 0.582 & 0.706 & 0.649 & 0.079 \\ -2.133 & 0.049 & -0.359 & -0.436 & -0.400 & -0.048 \\ 0.933 & -0.021 & 0.157 & 0.190 & 0.175 & 0.022 \end{pmatrix}$$

This has determinant 0.9999999951225 and eigenvalues

$$\begin{aligned} \lambda_1 &= 1503.58386741952 \\ \lambda_2 &= 1.00000696756 \\ \lambda_3 &= 0.96647413634 - 0.25676398461i \\ \lambda_4 &= 0.96647413634 + 0.25676398461i \\ \lambda_5 &= 0.99999303249 \\ \lambda_6 &= 0.00066507763 \end{aligned}$$

The determinant tell us we should not trust more than ten figures. Looking at the eigenvalues we see that two of the them are approximately unity as expected. Discarding these, the remaining eigenvalues describe the dynamics near the halo orbit, restricted to the energy level  $C_{halo}$ .

We have one very large, and one very small eigenvalue. We can in fact check that

$$1/\lambda_1 = 1/1503.58386741952 = 0.00066507763 = \lambda_6$$

so the real eigenvalues are reciprocal. This is as it should be since the flow preserves phase space volume. The eigenvectors corresponding to the stable and unstable eigenvalues direct us to the stable and unstable manifolds of the orbit. We will come back to this in the next section.

The remaining two eigenvalues  $\lambda_3$  and  $\lambda_4$  lie on the unit circle. These correspond to the center directions of the orbit. Then we expect there are orbits near the halo which remain near the halo for all time. These orbits are in fact in the center manifold of  $L_1$  as discussed above.

### 3.2 The Family of Halo Orbits at $L_1$

A periodic orbit in a Hamiltonian system is called *elementary* if its monodromy matrix has exactly two unity eigenvalues. For such a periodic orbit we have the following theorem (see [MH])

**Theorem 3 (The Cylinder Theorem)** *An elementary periodic orbit of a Hamiltonian system lies in a smooth cylinder of periodic solutions parameterized by the Hamiltonian integral.*

This proof uses the Poincaré map of the periodic orbit. If the orbit is elementary then this map has exactly one unity eigenvalue and application of the implicit function theorem gives a one parameter branch of fixed points for the map, that vary with energy.

Then having found one Halo Orbit and observing that it indeed has exactly two unity eigenvalues, we can use this as a starting place to move along the cylinder. We use the initial conditions of the halo orbit from above as a starting point to find a new halo orbit at a slightly larger value of  $x$  ( $x$  coordinate closer to the Earth). If we find another halo orbit here, we iterate the process. In this way we compute the cylinder from the theorem. The program which carries this out is “haloFamily.m”.

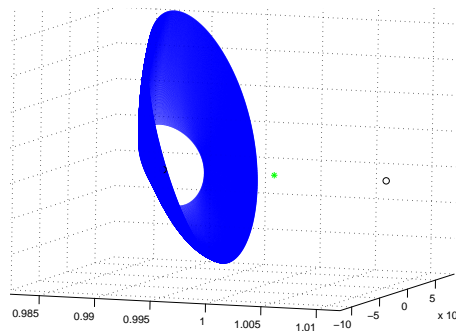


Figure 5: decreasing branch of the cylinder of halos

Figure 5 shows an annulus or cylinder of orbits. It is the branch in the direction of decreasing Jacobi Integral (which we sometimes call the Jacobi energy, or just energy). The orbits increase in diameter as they get close to earth. However their periods get shorter and shorter (this information is kept track of in the program). Then the trajectories nearer the earth move with greater velocity.

For energies lower than the right edge of the cylinder our Newton method loses track of the halo orbits, and begins to converge to a completely different family of orbits. By the cylinder theorem the halo orbits must cease to be elementary, and take on additional unity eigenvalues. This begs that we plot

the eigenvalues as a function of distance (energy) along the cylinder. In fact we plot the moduli of the eigenvalues in 6.

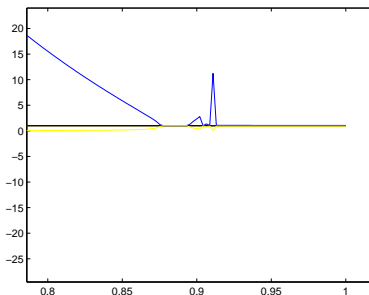


Figure 6: moduli of the eigenvalues of the halos

Each line is the value of the modulus of one of the eigenvalues, and it appears all but the blue are near or less than or equal to one throughout. The blue is the unstable eigenvalue and the plot suggests that its magnitude decreases steadily until it seems to reach one, and then it remains one for a short interval before behaving erratically and then returning to one.

The horizontal axis of the plot is just a normalized count of which orbit we are on, and has no physical units. Zero on this plot is the halo orbit, and one is the end of the computation, at which time the Newton method has converged to another family. Since the computation found 450 orbits total, one on the horizontal axis is the 450<sup>th</sup> orbit. From inspection of the program data we know that the Newton method loses the halo family near 0.9. So the graph seems to suggest that the new family is stable.

More interesting is the fact that the unstable direction seems to vanish for a brief time before the bifurcation. To see if this is really the case, we inspected by hand, the eigenvalues for orbits 390–400 and indeed find that for what seems to be an interval of halo orbits, before the breakdown, there are exactly two unity eigenvalues and four complex eigenvalues on the unit circle. This suggests the existence of stable halo orbits. Sure enough, one can choose initial conditions just off one of these halo orbits, and the resulting orbit remains bounded to it for several periods (possibly longer, we only integrated through 2).

What occurs on the second branch of the cylinder, when we increase the Jacobi Integral, is at least as interesting. How does the family of halo orbits die off in this direction? The evolution of the cylinder is shown in 7

It seems that the diameter of the cylinder decreases steadily, balancing the behavior in the other branch, and looks for a moment like it will simply close itself off around  $L_1$ . But the surface begins to warp and flatten itself down into the  $xy$ -plane. Then the halo orbits seem converge toward the Lyapunov family near  $L_1$ .

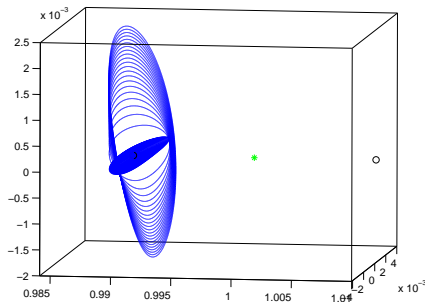


Figure 7: increasing branch

In fact the initial conditions of the 90<sup>th</sup> halo orbit are

$$\mathbf{x}_0 = \begin{bmatrix} 0.99019555537727 \\ 0 \\ 0.00000000000000 \\ 0 \\ -0.00148544716640 \\ 0 \end{bmatrix}$$

which is completely in plane. Further if we plot this orbit we see that it is in a  $10^{-3}$  neighborhood of  $L_1$  and looks elliptic. We do not show this picture as it is essentially the same picture we saw in the previous note set when examining the linearized dynamics about  $L_1$ .

But this suggests *post hoc*, a method which might find halo orbits. Recall that in order to find our first halo orbit we were given experimental data known to be close to a halo orbit. Instead we could have begun with an periodic orbit in the  $xy$ -plane from the linearized problem. We showed in the pervious set of notes that, in a  $10^{-3}$  neighborhood of  $L_1$ , these conditions are close to an in plane periodic Lyapunov orbit. Using this as a starting point we could then have constructed the cylinder of halo orbits, just as we have done here, only in reverse.

### 3.3 Family of Halo Orbits at $L_2$

Let's test the validity of this procedure at one of the other collinear libration points, say  $L_2$ . Beginning with the program 'linearDynamicsL2.m'(which is a small modification of 'problem5L1.m') and using the methods developed in the last set of notes, we find that the initial conditions

$$\mathbf{x}_{0lin} = \begin{bmatrix} 1.0102213775543 \\ 0.0 \\ 0.0 \\ 0.0 \\ -0.00085810939290 \\ 0.0 \end{bmatrix}$$

give a periodic orbit in the linearized dynamics at  $L_2$  with half period  $\tau_0 = 1.52727484975025$ . Again the pictures are not qualitatively different from those in the previous notes, so we suppress them.

Using  $\mathbf{x}_{0lin}$  and  $\tau_0$  as initial guesses in the program 'haloL2.m' (which is essentially the same as the program 'haloNewton3.m' that was used to find our first halo orbit) after six Newton steps the algorithm converges in the first twelve significant figures to a planar Lyapunov orbit near  $L_2$  with initial conditions

$$\mathbf{x}_0 = \begin{bmatrix} 1.01022137755430 \\ 0 \\ 0 \\ 0 \\ -0.00086783896829 \\ 0 \end{bmatrix}$$

and  $\tau_f = 1.52747206932445$ . Recall that the program holds the  $x$  coordinate fixed and adjusts the initial  $z$ ,  $\dot{y}$ , and  $\tau$ , and note the small differential correction in these variables.

Now, this orbit can be used as the starting point for the program 'haloFamilyL2.m', which is a modification of 'forwardHaloOrbits.m' designed to walk us backward from the initial orbit, toward the Earth. The results of this scheme are shown in fig 8

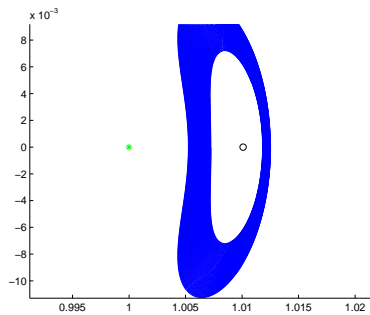


Figure 8: Cylinder of in plane orbits emanating from  $L_2$

The family of orbits so obtained is completely planar. We have found an interesting family of Lyapunov orbits, and we see that as we follow them toward the earth, they take on more and more of a kidney shape. Certainly this has not been a waste of time, but we don't yet have the halos at  $L_2$ .

Perhaps a modification of the strategy. The algorithm moves only the  $x$  coordinate and has the  $z, \dot{y}, \tau$  coordinates free. If we force the procedure out of plane near one or the larger Lyapunov orbits, will the procedure find a halo?

To this end we make the following modification to the program 'Newton3.m'. We begin with a large in plane Lyapunov orbit as the initial guess. Then fix a small  $z_0 > 0$  out of plane and let the Newton method search for  $x, \dot{y}$ , and  $\tau$  with  $z_0$  fixed. The program which carries out this scheme is 'haloNewtonL2.m'.

Begging with an in plane Lyapunov orbits as above, we choose somewhat arbitrarily, a primer orbit with initial conditions

$$\mathbf{x}_0 = \begin{bmatrix} 1.00675137755428 \\ 0 \\ 0 \\ 0 \\ 0.01867323092996 \\ 0 \end{bmatrix}$$

and initial half period  $\tau_0 = 3.23544384321752/2$ . This is used as the initial guess for the program 'haloNewtonL2.m' with the minor modification that we add an out of plane component  $z_0 = 0.0001$  as described above.

The results are exactly what we hoped. After 14 Newton iterations the program finds an out of plane orbit which is periodic to thirteen significant figures. The initial conditions the Newton scheme converges to are

$$\mathbf{x}_0^* = \begin{bmatrix} 1.00842815565444 \\ 0 \\ 0.0001 \\ 0 \\ 0.00981039306520 \\ 0 \end{bmatrix}$$

with  $\tau^* = 3.10262658029110$ , and plotting these shows that we have indeed found an out of plane periodic orbit near  $L_2$ .

Now, that we have such a halo orbit near  $L_2$  (which in fact has exactly two unity eigenvalues; we have checked this but don't give the numbers here) the cylinder theorem grants that the orbit is not isolated. There is a cylinder of halo orbits, and we hope to find it.

$\mathbf{x}_0^*$  gives a near plane halo. We hope to use this as a seed for the program 'haloFamilyL2.m' which will grow the cylinder and find large amplitude  $L_2$  halos.

The results are shown in 9. We see that we have indeed recovered a structure similar to that in fig 7 except now the orbits grow out of  $L_2$ , instead of collapsing

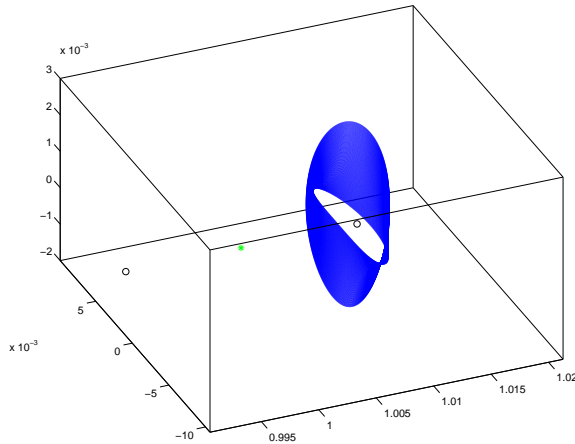


Figure 9: Cylinder of halo orbits emanating from  $L_2$

into  $L_1$ . Moreover we have built the cylinder in reverse; starting with an in plane orbit and arriving at halo orbits whose location we did not know even approximately before the computation.

This method is a vast improvement over the method used to compute the family of halos at  $L_1$ , where we were basically handed an initial condition close to some halo orbit. Using this scheme we should be able to find halo orbits near any of the collinear libration points, and at other values of  $\mu$ . Or at least we have an explicit process which *could* lead to results. We have not proven that the method always works, and some experimentation was involved in selecting an Lyapunov orbit to prime the computation. It would be nice to have a sound method for making this choice.

The state of the art for finding halo orbits is the method of normal forms described above, developed by Jorba, Simo, Masdemont, Gomez and others, and developed in [J]. On the other hand, the method of normal forms requires substantial computation time and complexity. For design purposes, and if one were in a hurry, the scheme described here might prove effective. (In fact I had a discussion with Masdemont which confirms that this is what people do).

## 4 Computing Stable and Unstable Manifolds of Periodic Orbits Through Linear Analysis

In the previous section we computed halo orbits and their linear stability using the monodromy matrix to approximate the linearization of the Poincare map

for the halo orbit. This linear analysis showed that many of the halo orbits have (one dimensional) stable and unstable directions. Then there are orbits which converge to the halo orbit in positive time, and orbits which converge to them in backward time.

Let  $o(\mathbf{x}_0^*) \doteq o_h$  denote the halo orbit. The set

$$W^s(o_h) = \{\mathbf{x} \in U : \phi(\mathbf{x}, t) \rightarrow o_h \text{ as } t \rightarrow \infty\}$$

is called the *stable manifold* of  $o_h$ . This set is non-empty by the linear analysis above. Similarly

$$W^u(o_h) = \{\mathbf{x} \in U : \phi(\mathbf{x}, t) \rightarrow o_h \text{ as } t \rightarrow -\infty\}$$

is the *unstable manifold* of  $o_h$  and again is non-empty. These are global objects by their definitions. By intersecting with a small enough neighborhood of the halo orbit we get the local stable and unstable manifolds. It can be shown that these are in fact smooth manifolds as the name suggests and that they are tangent to the stable and unstable eigenspaces near the halo orbit. Much more information about stable and unstable manifolds can be found for example in [MH], and [R].

For the moment it's enough to note that the linear analysis of the previous section, combined with the definition of the stable and unstable manifolds as the sets of points which flow to  $o_h$  in either forward or backward time, give us a practical method by which we can numerically compute these manifolds.

The method is simple, at least in principle. The orbit is one dimensional, with one unstable (*resp.* stable) direction. Then the unstable (*resp.* stable) manifold is two dimensional, and will be parameterized by two coordinates. In fact, the unstable (*resp.* stable) manifold can be shown to be foliated by unstable (*resp.* stable) orbits ([R]) hence is topologically (locally) a cylinder  $S^1 \times (R)$ , with angular coordinate parameterized by the halo orbit itself, and linear coordinate parameterized by time along the unstable (*resp.*) orbit.

For the angular coordinate we simply divide  $o_h$  up into  $N$  points  $\mathbf{x}_k^*$ ,  $1 \leq k \leq N$ . To each point there corresponds a time  $\tau_k$  such that  $\mathbf{x}_k^* = \mathbf{x}^*(\tau_k)$ , where here  $\mathbf{x}^*(t)$  is the halo orbit with initial condition  $\mathbf{x}_0^*$  found by the Newton method, i.e;

$$o_h = \{\mathbf{x}^*(t) : 0 \leq t < T\}$$

Let  $\xi_{u_0}$  (*resp.*  $\xi_{s_0}$ ) be the eigenvector associated with the unstable (*resp.* stable) eigenvalue of the monodromy matrix. These vectors are tangent to the unstable (*resp.* stable) manifold at  $\mathbf{x}_0^*$

It can in fact be shown that the stability type of the state transition matrix of any point  $\mathbf{x}_k^*$  on the halo orbit is independent of  $k$  and that the eigenvectors can be computed if the state transition matrix is known at a base point  $\mathbf{x}_k^*$ . They are just the eigenvectors of the monodromy matrix (which is computed at  $\mathbf{x}_0^*$ ) multiplied by the state transition matrix of the new point  $\mathbf{x}_k^*$ .

The relationship is

$$\xi_{u_k} = \Phi(0, \tau_k)\xi_{u_0}$$

and

$$\xi_{s_k} = \Phi(0, \tau_k)\xi_{s_0}$$

where  $\xi_{u_k}$  (*resp*  $\xi_{s_k}$ ) is tangent to the unstable (*resp* stable) manifold at  $\mathbf{x}_k^*$ .

Then for each  $\mathbf{x}_k^*$  we compute the state transition matrix  $\Phi(0, \tau_k)$  and from this obtain the tangent space to the stable and unstable manifolds there, by the formulae above. Set a tolerance  $\epsilon$ . If  $\epsilon$  is small enough then

$$\mathbf{x}_{u_k}(0) = \mathbf{x}_k^* \pm \epsilon \xi_{u_k}$$

and

$$\mathbf{x}_{s_k}(0) = \mathbf{x}_k^* \pm \epsilon \xi_{s_k}$$

are points very nearly on the unstable (*resp* stable) manifolds. We integrate these initial conditions over some time interval  $[0, T_f]$  obtaining the orbits  $\mathbf{x}_{s_k}(t)$ . Then  $t$  along these orbits is the second coordinate on the manifold. By varying  $k$  and  $t$  we obtain a good approximation of the manifolds.

#### 4.1 The Stable and Unstable Manifolds of the $L_1$ Halo Orbit

The procedure described in the previous sub-section is carried out by the programs *positiveBranch.m*, *negativeBranch.m*, *unstablePositiveBranch.m*, *unstableNegativeBranch.m*, which compute the positive and negative branches of the stable and unstable manifolds of the halo orbit that was found by the Newton method in the previous section.

The halo orbit is parameterized by 100 points. Fig 10 gives a look at the branch of the stable manifold on the Earth side of  $L_1$  (manifold is blue). The earth (which is hard to see as the manifold wraps around it) is a green star, the halo orbit itself is the black loop, and  $L_1$  is the black star. We have plotted the zero velocity surface associated with the orbit so that it's position and the embedding of it's stable manifold can be seen with reference to the neck.

We took  $\epsilon = 2 \cdot 10^{-8}$  and parameterized the unstable orbits by  $t \in [0, 2.25 \cdot T]$  where  $T$  is the period of the halo orbit. Because the halo orbit is so large, the manifold takes up a lot of space in the Earth's energy cavity.

Fig 11 shows a close up of the same manifold and parameterized over a shorter time interval. Here you can just see the Earth as a red star in the middle of the picture (where the embedding stable manifold seem be wrapping the most). It's not clear what the exact geometry of the embedding it. However it is clear that the stable manifold passes very near the earth.

This kind information has can be very useful for mission design. To send a satellite to the halo orbit, one designs an orbit which goes from a low earth

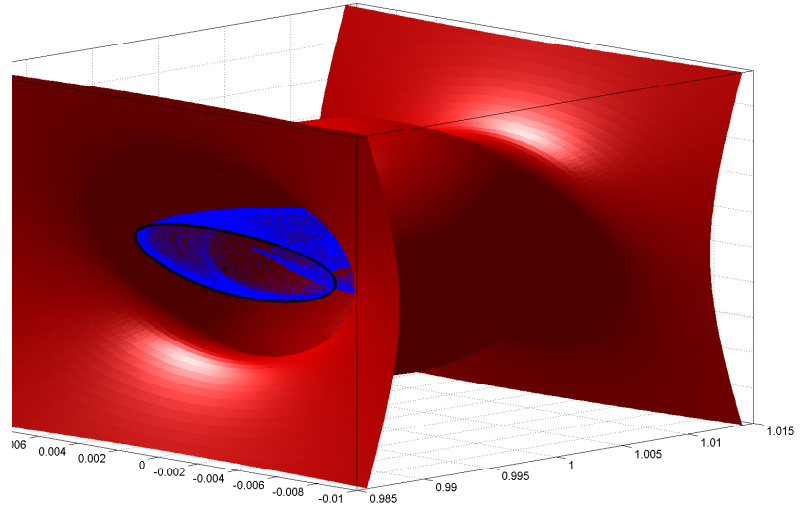


Figure 10: Stable Manifold of the Halo Orbit; Secondary Body Branch

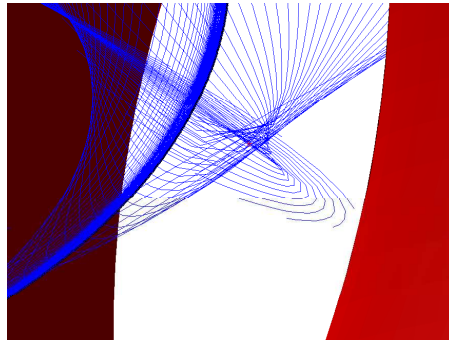


Figure 11: Stable Manifold of the Halo Orbit

orbit, to the stable manifold of the halo. Then the satellite will be carried by the dynamics of the stable manifold to the halo orbit, as the dynamics on the stable manifold is gradient-like.

Fig 12 shows the other branch of the stable manifold. This is obtained by taking initial conditions scaled by minus one times the stable eigen vector. This branch goes away from the secondary body, out toward the (primary) Sun, which is shown in the middle as a red star. This integration time used was much longer as this branch of the manifold extends through a much larger portion of

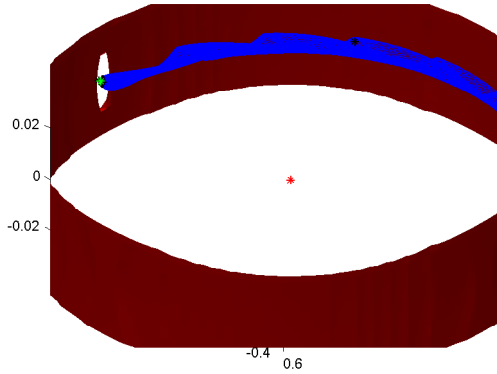


Figure 12: Stable Manifold of Halo Orbit; Primary Body Branch

phase space.

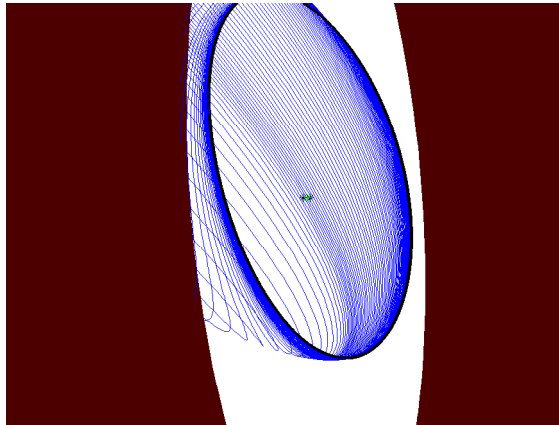


Figure 13: Stable Manifold of Halo Orbit; Close Up Near  $L_1$

The same manifold is shown in 13. This time we take a closer look, integrating over a shorter time, and from a new angle. This view highlights tube like structure of the invariant manifold.

Now we look again at the global picture but with the unstable manifold plotted as well. This is Fig 14. We see that opposite  $L_1$  near  $L_3$  the manifolds seem to intersect. If they do, as the picture suggests, this would imply the existence of an orbit which goes to the halo in forward time, and comes from it in backward time. Such an orbit is called a homoclinic connection.

Such an intersection is a strong indicator of interesting dynamics. If the

intersection exists and is non-degenerate enough (say transverse intersection or even just 'topological crossing') this implies the existence of very complex 'chaotic' dynamics ([GR]).

In that paper it is shown that one can find orbits which "shadow" the dynamics on the halo orbit (which is an invariant torus in the center manifold of  $L_1$ ) and then "shadow" the unstable manifold to the intersection with the stable manifold. Then the stable manifold can be followed back to the halo.

Again, if certain non-degeneracy conditions are satisfied then there is a region of phase space, near the halo, on which the dynamics are topologically semi-conjugate to symbolic dynamics. In short this means that there exist trajectories that shadow the halo as many times as you like, then traverse homoclinic connection, then orbit the halo any other number of times we like.

The presence of symbolic dynamics implies the existence of orbits corresponding to any sequence of ones and zeros, where a one in the sequence means going around the halo orbit, and a zero means going around the homoclinic connection. So if you pick the sequence 00110101..., then there exists an orbit which goes around the connection twice, then around the halo once, then alternates around the connection and then the halo, and so on.

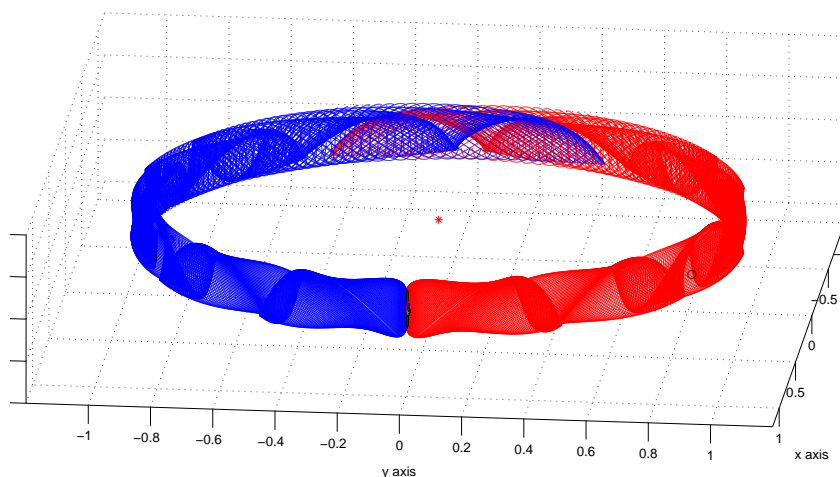


Figure 14: The Primary Side Branches of the Stable (blue) and Unstable (red) Manifolds

Fig 15 shows the intersection of the stable and unstable manifolds at the halo orbit. It should be noted that in the phase space the manifolds only intersect at the halo (at least this close to the halo orbit, if they truly intersect in the phase space it is probably closer to  $L_3$ ). The manifolds are two dimensional objects which embed properly into six dimensional space. It is only when we project them into the three dimensional configuration space that they seem to

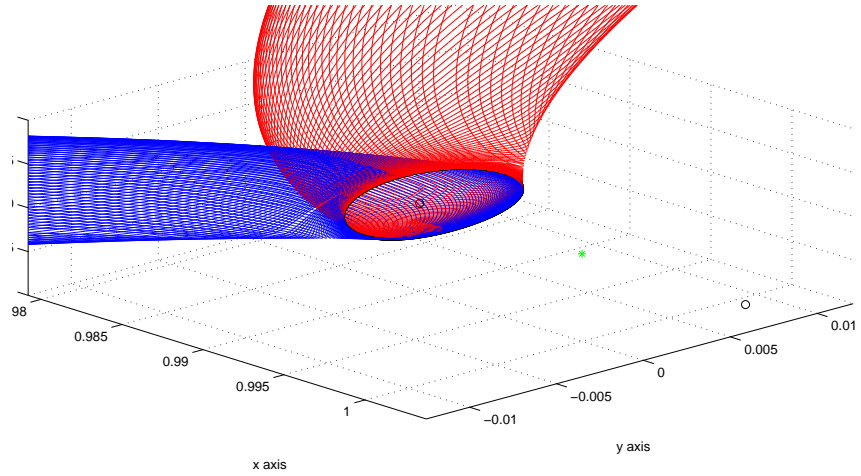


Figure 15: The Primary Side Branches of the Stable (blue) and Unstable (red) Manifolds: Intersection at the Halo

intersect.

A similar observation is that putting an projectile “on” the stable manifold involves not just getting the projectile to a certain point in configuration (physical) space, but also getting it there with the right velocity. The stable and unstable manifolds are not just subsets of the configuration space, but instead are subsets of the full tangent or cotangent bundle.

## 4.2 Other Periodic Orbits

In this section we will look for a couple of other periodic orbits, and imitate the above analysis on these, in order to illustrate that the utility of the methods developed in the previous sections are not at all limited to the study of halo orbits.

## 4.3 Stable and Unstable Manifolds of the Lyapunov Orbits

Consider a Lyapunov orbit about  $L_1$  in the Earth/Moon system. By using the Linear analysis from the previous set of notes and a modification of the Newton method developed in these notes, we find that the initial conditions

$$\mathbf{x}_0 = \begin{pmatrix} 0.83946302646687 \\ 0 \\ 0 \\ 0 \\ -0.02596831282986 \\ 0 \end{pmatrix}$$

produce an orbit about  $L_1$  which is periodic to 12 significant figures, has period  $T = 2.69239959528586$ , and energy  $C = 3.18894909055242$ . The orbit is shown in fig 16

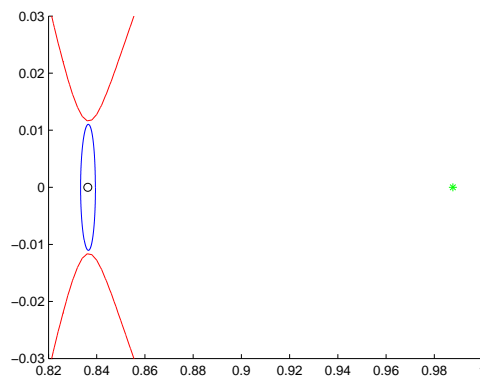


Figure 16: A Lyapunov Orbit

Linear stability analysis shows that the orbit has a stable and unstable direction, a two dimensional center, and of course two unity eigenvalues when considered as an orbit in the spatial problem. In the planar problem the orbit is purely unstable.

Now we will compute the stable and unstable manifolds of this orbit. Since the problem is planar this will produce nicer pictures than the pictures of the stable and unstable manifolds of the halo orbits above (or at least pictures easier to read).

The procedure is exactly as before. In fact we use the program ‘unstable-PositiveBranch.m’ which actually computes the stable branch in forward time. This program was designed to compute the stable manifold of the halo orbit, but it computes the stable manifold for the Lyapunov orbit just as easily. The only change that needs to be made is that the data above is entered, instead of the halo orbit data. The branch of the stable manifold which encloses the Moon is shown in fig 18, while the unstable branch is in fig

The fact that the stable and unstable manifolds obviously intersect several times in the configuration space begs the question whether they intersect in the phase

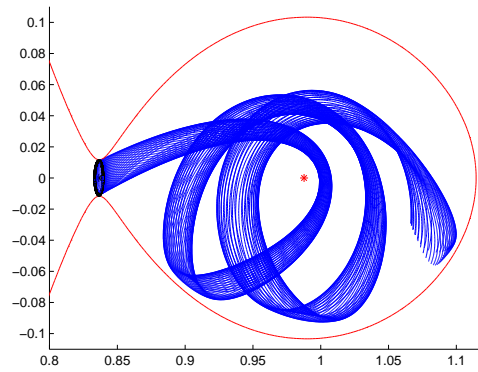


Figure 17: The Stable Manifold of the Lyapunov Orbit about the Moon

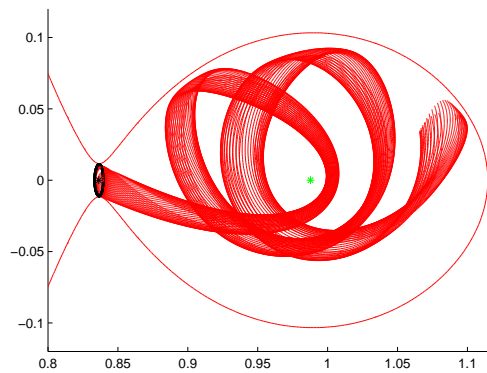


Figure 18: The Un-Stable Manifold of the Lyapunov Orbit about the Moon

space. If they do, then the Lyapunov orbit has a homoclinic connection and gives rise to complicated dynamics. This will make the subject of a future set of notes, but for now we simply cite [J]

## References

- [A] Methods of Applied Mathematics, Unpublished Notes:  
[www.math.utexas.edu/~arbogast/](http://www.math.utexas.edu/~arbogast/)
- [GR] Marian Gidea, Clark Robinson, “Symbolic Dynamics for Transi-

tion Tori-II", Qualitative Theory of Dynamical Systems 1, 1-14  
(2000) Article No.1

[HS] Morris W. Hirsch, Stephen Smale, Differential Equations, Dynamical Systems, and Linear Algebra, Academic Press

[J] Angel Jorba, Carles Simo, Josep Masdemont, Gerard Gomez, Dynamics and Mission Design Near Libration Points, Vol. III, Advanced Methods for Collinear Points, World Scientific Publishing Co, 2001.

[MH] K.R. Meyer, G.R. Hall, Introduction to Hamiltonian Dynamical Systems and the N-body Problem, Springer-Verlag

[R] Clark Robinson, Dynamical Systems: Stability, Symbolic Dynamics, and Chaos, Second Edition, CRC Press, Boca Raton Florida, 1999